Electrostatic origin of *in vitro* aggregation of human γ-crystallin

Benjamin G. Mohr,[1] Cassidy M. Dobson,[2] Scott C. Garman,[2]
and Murugappan Muthukumar[1,a)]
[1]*Department of Polymer Science and Engineering, University of Massachusetts, Amherst, Massachusetts 01003, USA*
[2]*Department of Biochemistry and Molecular Biology, University of Massachusetts, Amherst, Massachusetts 01003, USA*

(Received 27 March 2013; accepted 8 July 2013; published online 29 July 2013)

The proteins α-, β-, and γ-crystallins are the major components of the lens in the human eye. Using dynamic light scattering method, we have performed *in vitro* investigations of protein-protein interactions in dilute solutions of human γ-crystallin and α-crystallin. We find that γ-crystallin spontaneously aggregates into finite-sized clusters in phosphate buffer solutions. There are two distinct populations of unaggregated and aggregated γ-crystallins in these solutions. On the other hand, α-crystallin molecules are not aggregated into large clusters in solutions of α-crystallin alone. When α-crystallin and γ-crystallin are mixed in phosphate buffer solutions, we demonstrate that the clusters of γ-crystallin are prevented. By further investigating the roles of temperature, protein concentration, pH, salt concentration, and a reducing agent, we show that the aggregation of γ-crystallin under our *in vitro* conditions arises from non-covalent electrostatic interactions. In addition, we show that aggregation of γ-crystallin occurs under the dilute *in vitro* conditions even in the absence of oxidizing agents that can induce disulfide cross-links, long considered to be responsible for human cataracts. Aggregation of γ-crystallin when maintained under reducing conditions suggests that oxidation does not contribute to the aggregation in dilute solutions. © *2013 AIP Publishing LLC*. [http://dx.doi.org/10.1063/1.4816367]

I. INTRODUCTION

Uncontrolled aggregation of protein molecules is widely recognized as one of the underlying macromolecular features of various diseases. A specific example is the formation of cataract in the lens of human eye.[1] In general terms, the proteins constituting the lens aggregate over a period of time due to damage from exposure to radiation, chemical reactions, and noncovalent forces.[2] These aggregates become insoluble and obstruct light from reaching the retina by scattering the incident light.[3] Although it is well established that cataracts consist of insoluble aggregated lens proteins, the precise molecular mechanism of cataract formation is unclear.[4] One of the fundamental issues in this context is the nature of intermolecular interactions among the various constituent proteins in the lens.

The lens is primarily made of crystallin proteins (about 90% of the total protein content) at high concentrations of 200–450 mg/ml, and there are two main classes of crystallins:[5] (i) α-crystallins which are responsible for structure and chaperoning and (ii) β- and γ-crystallins which are primarily structural.[6] α-crystallin proteins account for nearly 50% of the lens protein mass, and are found in a 3:1 ratio with β- and γ-crystallins.[4,7] The α-crystallin family consists of αA- and αB-crystallins, which have about 60% amino acid sequence identity.[8] Analogous to their homologous small heat shock proteins such as hsp20, the α-crystallins have been shown to form polydisperse oligomers with masses ranging between 300 and 1200 kDa.[9,10]

While the β-crystallins are capable of forming dimers as well as homo- and hetero-oligomers, the unaggregated γ-crystallins are monomers in the eye.[11] The human γ-crystallin family consists of five members, the γA-, γB-, γC-, γD-, and γS-crystallins, which are highly similar in sequence and molar mass of about 21 kDa.[12] The γA-crystallins–γD-crystallins are expressed early in lens development and are primarily found in the lens core, where γC- and γD-crystallins are the most prevalent. γS-crystallin is produced in later development and is thus more prevalent in the periphery of the lens.[13]

According to one model, the transparency of the lens without cataract formation is due to regular arrangements of various protein molecules in the lens.[1,14] Over decades of aging, the protein arrangement in the lens is disrupted by the aggregation of crystallins, due to damage from many contributing factors including ultraviolet radiation, deamidation, glycation, and methylation.[15–20] One model for defense against cataract formation, buttressed by experimental data, is that α-crystallin protects the β- and γ-crystallins from aggregation by binding denatured proteins.[21] When the protective effect of α-crystallin is overwhelmed, the concentration of denatured β- and γ-crystallins can rise to a critical level where aggregation begins.[22–24] Eventually these aggregates become insoluble and cataracts occur. Insoluble cataract tissue can be solubilized in the presence of the denaturing agent 6M guanidine hydrochloride and the reducing agent 1M dithiothreitol (DTT), suggesting that both noncovalent

a)Author to whom correspondence should be addressed. Electronic mail: muthu@polysci.umass.edu

interactions and disulfide bonds are relevant in cataract formation.[25]

As an alternative mechanism of cataract opacity, extensive quasielastic light scattering investigations[3,26–30] in the context of *in vivo* cold cataract have shown that cataract opacity is due to critical opalescence and not aggregation. The fluctuations in the protein concentration have been shown to lead to scattered light. In the absence of cataract, the lens proteins have liquid-like order and the protein-protein interactions suppress concentration fluctuations, instead of the initially hypothesized regular array of proteins.[1,14] The role of calcium ions in affecting the cataract formation has also been investigated[31–34] in calf lens cytoplasmic extracts.

A large body of literature is devoted to understanding the intermolecular interactions among α-, β-, and γ-crystallins. The chaperone property of α-crystallins on the deaggregation of γ- and β- crystallin aggregates has been well established.[21,35–40] Details on the specific sites of the crystallin molecules responsible for aggregation and deaggregation have also been addressed by several research groups.[41–49]

Despite the huge progress briefly mentioned above, the nature of intermolecular forces among crystallin proteins still remains elusive from a full understanding. The primary objective of the present paper is to explore the interactions of γ-crystallin molecules in very dilute *in vitro* buffer solutions under varying conditions. The experimental conditions used in the present study are not at all reminiscent of *in vivo* systems, but are chosen to understand the chemical physics of these proteins.

Dynamic light scattering (DLS) is a sensitive technique to monitor the formation of aggregates and dynamics of concentration fluctuations in dilute solutions of macromolecules. Using DLS, we have investigated the scattering properties in solutions of crystallins. Among the various crystallins briefly listed above, we have chosen γD- and γS-crystallins (due to their abundance and locations in the lens), and αA- and αB-crystallins (because of their chaperoning effect) in our investigation. These proteins were produced by cloning and expressing recombinant human αA-, αB-, γD-, and γS-crystallins. We have studied the effects of composition and concentration of the proteins, temperature, pH, and ionic strength on the light scattering of dilute solutions far away from concentrations pertinent to *in vivo* systems. As detailed below, DLS shows the spontaneous formation of aggregates of γ-crystallin molecules which coexist with unassociated monomers. Our results show that these aggregates are destabilized in the presence of α-crystallin molecules. In addition, we have addressed the issue of whether disulfide cross-links are present in the aggregates of γ-crystallin by treating the aggregates with the reducing agent DTT. We have found that the aggregates persisted even in the presence of DTT. While the temperature did not significantly alter the aggregates, high pH and higher ionic strength led to the disappearance of the aggregates of γ-crystallin. Based on our *in vitro* observations, we conclude that non-covalent electrostatic interactions among the protein molecules are responsible for the aggregation of γ-crystallin. Our research provides additional insight into mechanisms of γ-crystallin aggregation in dilute solutions.

The rest of the paper is organized as follows. The materials and the experimental methods are described in Sec. II. The dynamic light scattering data on solutions of crystallins under various experimental conditions are presented in Sec. III along with discussions. The main conclusions are summarized in Sec. IV.

II. MATERIALS AND METHODS

A. Cloning, expression, and purification of human αA-, αB-, γD-, and γS-crystallins

The recombinant plasmids separately containing the genes for αA-, αB-, γD-, and γS-crystallins (kindly provided by Dr. Jonathan King at MIT (Cambridge, MA, USA)) were first amplified in the TAM1 *E. coli* cell line, followed by purification with PureYield Plasmid Miniprep System (Promega, WI). The plasmids for γD- and γS-crystallins donated by Dr. Jonathan King already contained an N-terminal hexahistidine tag needed for purification of the protein. For the plasmids of αA- and αB-crystallins, we added an N-terminal hexahistidine tag with a tobacco etch virus (TEV) protease site by PCR. For the Polymerase Chain Reaction (PCR), we used 1–2 μl of the recombinant plasmid, 0.5 μl of Phusion High Fidelity DNA Polymerase (New England BioLabs, MA), 1 μl of 10 mM dNTPs (New England BioLabs, MA), 1 μl of forward primer, and 1 μl of reverse primer with the total volume of 50 μl. The forward primer and the reverse primer for the αA-crystallin are, respectively, (5′-ACCAT CACCATCACCATGAGAACCTTTATTTTCAGGGCGACG TGACCATCCACCACCCC-3′) and (5′-CATATGTATATC TCCTTCTTAAAGTTAAACAAATTATTTCTAGAGGG-3′) (Fisher Scientific, NH). The forward and the reverse primers for the αB-crystallin are, respectively, (5′-CACCATCACCAT CACCATGAGAACCTTTATTTTCAGGGCGACATCCGCC ATCCACCA-3′) and (5′-CATATGGGCTATGTATATCTCCT TCTTAAAGTTAAC-3′) (Fisher Scientific, MH). Presence of the correct sequence in each construct was confirmed by DNA sequencing (Genewiz, South Plainfield, NJ).

The recombinant plasmids containing the histidine tags were transformed into protein expression *E. coli* cell lines as previously described.[50] αA- and αB-crystallins were expressed in BL21 bacterial cells (Novagen, WI), whereas γD- and γS-crystallins were expressed in M15[pRep4] cells (Qiagen, MD). Cells were lysed by conventional methods and the proteins were purified by a combination of nickel affinity and cation-exchange chromatography. The purity and size of each protein were confirmed by Sodium Dodecyl Sulfate Polyacrylamide Gel Electrophoresis (SDS-PAGE).

Proteins were then dialyzed into 150 mM NaCl, 20 mM Na_2HPO_4/NaH_2PO_4 buffer (pH 6.8). All salts were purchased from Fisher Scientific. Protein concentrations were calculated by absorbance at 280 nm using protein extinction coefficients of αA-crystallin 14.57 cm^{-1} M^{-1}, αB-crystallin 13.98 cm^{-1} M^{-1}, γD-crystallin 41.04 cm^{-1} M^{-1}, and γS-crystallin 41.59 cm^{-1} M^{-1}.

B. Dynamic light scattering

Dynamic light scattering measurements were made using an ALV goniometer instrument which had an ALV-5000/E

correlator equipped with 288 channels (ALV, Langen Germany) and a 2 W argon laser (Coherent Inc., Santa Clara, CA) with a working power of approximately 40 mW. Scattering intensity was measured at angles between 30° and 90° at 5° intervals, corresponding to a scattering wave vector (q) range between 8.41×10^6 and 2.30×10^7 m^{-1}. The scattering wave vector is defined as $q = 4\pi n \sin(\theta/2)/\lambda$, where θ is the scattering angle, and $\lambda = 514.5$ nm, the wavelength of the argon laser in vacuum, and n is 1.33, the refractive index of water. The temperature of the sample was held at various constant temperatures with an accuracy of ±0.1 °C by a circulating water bath.

The spatially averaged intensity-intensity correlation function $g_2(t)$, with t being the lag time between the measured intensities, is related to the field correlation function $g_1(t)$ by the Siegert relation,[51]

$$g_2(t) = B(1 + \beta \mid g_1(t) \mid^2), \tag{1}$$

where B is a baseline and β depends on the beam radius and aperture radius of the detector. For ideal situations of isolated scattering molecules undergoing Brownian motion in dilute solutions, $g_1(t)$ is a single exponential,[52]

$$g_1(t) = \exp(-\Gamma t) = \exp(-t/\tau), \tag{2}$$

with the decay rate Γ and the decay time τ given in terms of the diffusion coefficient D by

$$\Gamma = Dq^2; \quad \tau = \frac{1}{Dq^2}. \tag{3}$$

The diffusion coefficient is related to the hydrodynamic radius R_h of the scattering molecule by assuming the validity of the Stokes-Einstein relation,

$$D = \frac{k_B T}{6\pi \eta R_h}, \tag{4}$$

where $k_B T$ is the Boltzmann constant times the absolute temperature, and η is the viscosity of the solvent. By combining Eqs. (1)–(4), the hydrodynamic radius of the molecule is inferred from the measured $g_2(t)$.

In reality, when $g_1(t)$ is obtained from the experimentally measured $g_2(t)$ after accounting for B and β, it is usually not a single exponential decay. It is usually a sum of multiple exponentials with varying weights for these exponential decays. In general, $g_1(t)$ is represented as

$$g_1(t) = \int w(\Gamma) e^{-\Gamma t} d\Gamma. \tag{5}$$

The inverse Laplace transform of $g_1(t)$ according to the above equation yields the distribution function $w(\Gamma)$ in terms of the decay rate Γ. From this, the distribution function $A(\tau)$ of the decay times is obtained. By imposing the relation between the decay time and the hydrodynamic radius as given by Eqs. (3) and (4), the average size and the size distribution function are inferred from $A(\tau)$. In general, the analysis of $g_1(t)$ in systems with several decay rates is a difficult task and many protocols have been suggested over the years.[53,54] Among these methods of data analysis, we have used the CONTIN method and multi-exponential fitting procedure. Details of these procedures are given in Refs. 53 and 54, respectively. Measurements were typically run for 30 s (much longer than the characteristic times for diffusion) and repeated 3 times for CONTIN analysis and 10 times for multi-exponential analysis. For CONTIN analysis, each data set was individually analyzed and the results were averaged. For the multi-exponential analysis, the correlation functions were averaged, which provides a single averaged result.

Typically, the CONTIN analysis of DLS data for our system shows that a plot of the distribution function $A(\tau)$ versus τ exhibits one or more peaks for each scattering angle θ (defining the scattering wave vector q). This inference is also corroborated by the multi-exponential analysis. We identify each of these peaks as separate modes of dynamics. We then track each of these modes at the various scattering angles and construct their decay rates as a function of q. The q-dependence of the decay rate Γ (for each of these modes) is plotted as Γ vs. q^2. As suggested by Eq. (3), the slope of this plot is the diffusion coefficient for the particular mode. After ensuring that the decay rate is quadratic in q (corresponding to purely diffusive motion of the scattering molecule or aggregate), we obtain the value of R_h for each of the modes from the slope thus obtained and Eq. (4). We get similar values of R_h based on the multi-exponential analysis as well.

The DLS measurements were performed on the individual αA-, αB-, γD-, and γS-crystallin protein solutions with an initial concentration of 1.0 mg/ml, at 37 °C, in 150 mM NaCl, 20 mM Na_2HPO_4/NaH_2PO_4 buffer (pH 6.8). All solutions were filtered with 0.22 μm hydrophobic Polyvinylidene Difluoride (PVDF) membranes (Fisher Scientific) into 10 mm diameter borosilicate glass tubes and sealed. Solutions were allowed to equilibrate for an hour at 37 °C prior to DLS measurements. Subsequently, the αA- and αB-crystallins were each individually mixed with γD- and γS-crystallins in a molar ratio of 3:1, respectively, mimicking the ratio found in the human eye lens. All solutions were allowed to equilibrate for an hour at 37 °C before being filtered (0.22 μm hydrophobic PVDF membranes) into 10 mm diameter borosilicate glass tubes and sealed.

The γ-crystallin solutions were separately subjected to a variety of experimental conditions, including a range of temperatures (4 °C, 22 °C, 37 °C), dilutions (0.5 mg/ml, 1.0 mg/ml, 1.5 mg/ml, 2.0 mg/ml, 3.0 mg/ml, 4.0 mg/ml), reducing agent (5 mM DTT), concentrations of NaCl (100 mM, 150 mM, 300 mM, 400 mM, 500 mM, 1000 mM), and pH (5, 6, 7, 8, 9, 10, 11). Unless specifically mentioned, the γ-crystallin concentration was 1.0 mg/ml, at 22 °C, in 150 mM NaCl, 20 mM Na_2HPO_4/NaH_2PO_4 buffer (pH 6.8) and filtered with 0.22 μm hydrophobic PVDF membrane. Samples were allowed to equilibrate for 1 h at 22 °C prior to measuring light scattering. Temperature was controlled via a circulating water bath. After the desired temperature was achieved the sample was allowed to equilibrate at that temperature for an additional hour. Desired weight fraction was achieved by serial dilution. All samples for dilution were filtered with 0.80 μm hydrophobic PVDF membranes (Fisher Scientific). The 5 mM DTT environment was achieved using a 1M stock solution of DTT (Sigma Aldrich). Salt concentration and pH were adjusted via repeated dialysis (5l, 3 times over 24 h, 6 000–8 000 Molecular Weight Cut Off (MWCO)) at 4 °C and their final concentration adjusted to

1.0 mg/ml. For solutions with pH 5–8, a Na_2HPO_4/NaH_2PO_4 buffer was used, and for solutions with pH 9–11, a glycine buffer ($C_2H_5NO_2$/NaOH) (Fisher Scientific) was used.

C. Static light scattering

We have used the standard Zimm analysis[52] of the scattered intensity measured at various scattering angles θ and protein concentrations c on solutions, prepared as described above, to obtain the radius of gyration R_g, apparent molar mass M, and the second virial coefficient A_2. The same ALV instrument used for DLS was used here as well. A plot of inverse scattering intensity ($=Kc/R$, with K being the appropriate constant for the apparatus and R the Rayleigh ratio) is constructed at different values of θ and c. These data are then extrapolated to the limit of $c \rightarrow 0$, and the slope and the intercept of the straight line for Kc/R versus $\sin^2(\theta/2)$ yield R_g and M. The slope of the extrapolated line, in the limit of $\theta \rightarrow 0$, for Kc/R versus c yields A_2. In our data analysis we have assumed that the refractive index increment of the solution due to protein concentration is 0.196.[57] We performed static light scattering analysis for only α-crystallin solutions as only these solutions exhibited a single mode of concentration fluctuations in DLS.

D. Analytic size exclusion chromatography

All samples were prepared at a final concentration of 0.2 mg/ml in 150 mM NaCl and 20 mM Na_2HPO_4/NaH_2PO_4 buffer (pH 6.8). The γD- and γS-crystallin solutions were placed at 37 °C and allowed to air oxidize over a period of four days. Samples were injected with an initial concentration of 0.2 mg/ml, collected and subsequently re-injected after 24, 48, and 96 h. The γD- and γS- crystallin solutions were also subjected to chemical oxidation for 14 h with 0.1 mM $CuCl_2$ (Sigma Aldrich, MO) at 37 °C.

The samples were analyzed by Superose 6 HR 10/30 column (General Electric Healthcare, WI) equilibrated with Na_2HPO_4/NaH_2PO_4 buffer (pH 6.8) and 150 mM NaCl. Experiments were conducted at 4 °C with a flow rate of 0.5 ml/min. Molecular weight standards were used to calibrate elution times for the various protein sizes (17.6 kDa myoglobin, 66 kDa albumin, 669 kDa thyroglobulin, 2000 kDa blue dextran—Sigma Aldrich, MO). Fractions were collected and the presence of protein was confirmed by SDS-PAGE analysis.

III. RESULTS AND DISCUSSION

The strategy behind our DLS measurements is the following. First, solutions containing only one component of the four proteins (γD-, γS-, αA-, and αB- crystallins) were investigated. As shown below, solutions of either γD or γS exhibited two modes in DLS. The sizes inferred from these two modes correspond to unaggregated and aggregated forms of these proteins. On the other hand, solutions of either αA- or αB-crystallins exhibited only one mode in DLS corresponding to only one unaggregated but oligomeric population with slight polydispersity. Next, we mixed γ- and α-crystallins in the 1:3 ratio by weight, in order to assess the interference of α-crystallins on the spontaneous aggregation of γ-crystallins. Indeed, we find that the aggregates of γ-crystallins are absent in the presence of α-crystallins. After demonstrating this effect, we proceeded to evaluate the possible origin of aggregation in γ-crystallin solutions by monitoring the effects from variations in salt concentration, pH, protein concentration, temperature, presence of the reducing agent DTT and the oxidizing agent $CuCl_2$, and air oxidation. All DLS data reported here suggest that the spontaneous aggregation of γ-crystallins arises from non-covalently bonded electrostatic interactions among the protein molecules.

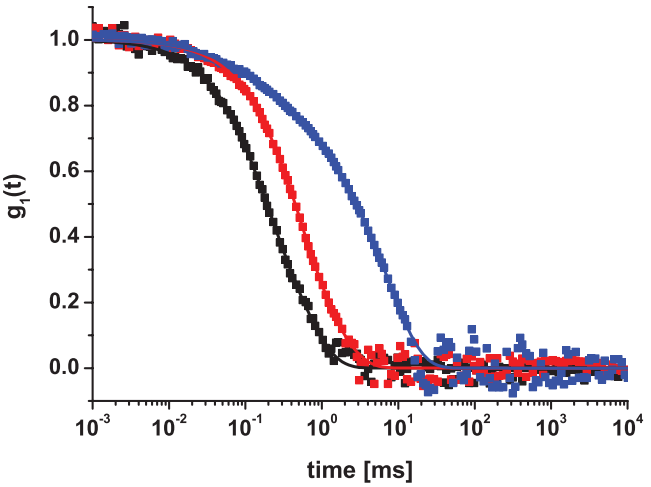

FIG. 1. Dependence of the field correlation function on lag time for solutions containing (a) γS-crystallin (blue), (b) αB-crystallin (black), and (c) γD- and αB-crystallins (red), at the scattering angle of 30°.

A. Spontaneous aggregation in γ-crystallin solutions

The DLS measurements were performed on individual solutions of γS- and γD- crystallins with the protein concentration of 1.0 mg/ml and 150 mM NaCl at 37 °C and pH 6.8 (20 mM N_2HPO_4/NaH_2PO_4). As a typical result, the field correlation function $g_1(t)$ (t being the lag time) for γS-crystallin solutions is given in Fig. 1 at the representative scattering angle of 30°. (For later comparisons, data from solutions of α-crystallin and mixtures of γ- and α-crystallins are also included in Fig. 1.) The CONTIN analysis at the various scattering angles investigated yields the distribution function of the decay time for each of the scattering angles as shown in Fig. 2(a). It is clear from Fig. 2(a) that there are two modes in the distribution function for each of the scattering angles. By following the procedure outlined in Sec. II, the decay rates of these two modes are obtained as a function of the scattering wave vector q. One decay rate is in the range of 10^4 s^{-1} and the other in the range of 10^3 s^{-1}. The dependencies of these rates on the scattering wave vector are given in Figs. 3(a) and 3(b), respectively. It is clear from the linear relation between the decay rate Γ and q^2 in these figures that both decay modes follow purely diffusive behavior, as also corroborated by multi-exponential analysis

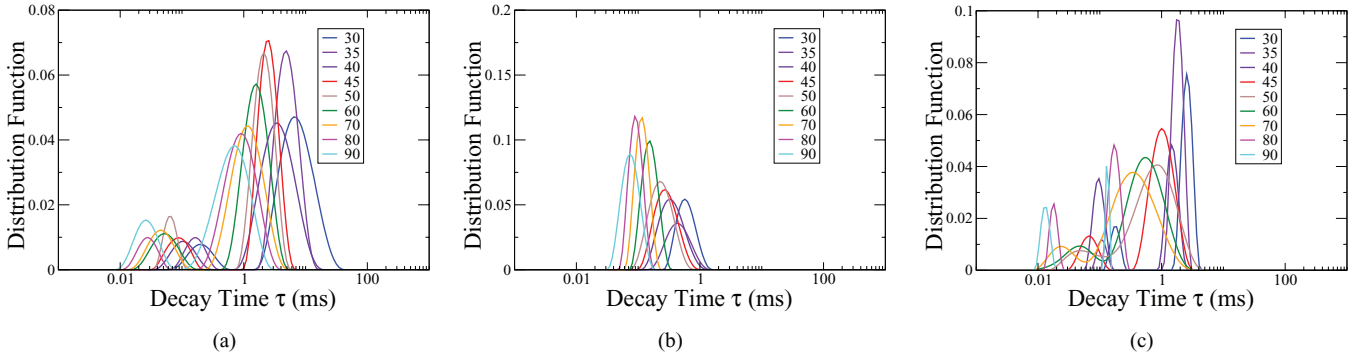

FIG. 2. Distribution function versus decay time at various scattering angles. (a) γS-crystallin solution exhibiting two modes at each scattering angle. (b) αB-crystallin solution exhibiting only one mode at each scattering angle. (c) Mixture of γS- and αB-crystallins exhibiting one mode each for the constituents without any representation from aggregated forms of γS-crystallin.

(not shown). From the slopes, we get the diffusion coefficients. The nice separation of time scales in Fig. 2(a) and between Figs. 3(a) and 3(b) suggests that there are two kinds of populations in γS-crystallin solutions, as also confirmed by multi-exponential analysis. The larger slope associated with the faster decay rate variations in Fig. 3(a) corresponds to a higher diffusion coefficient and consequently smaller hydrodynamic radius R_h (in view of Eq. (4)). Similarly, the smaller slope in Fig. 3(b) corresponds to a larger hydrodynamic radius. The values of R_h representing the most probable sizes of the two populations in γS-crystallin solutions are 2.6 $\pm$ 0.2 nm and 95 $\pm$ 8 nm, respectively (Table I). The multi-exponential analysis of the same data shows two populations with R_h values of 3.4 nm and 113 nm (Table I).

We attribute these two sizes obtained from the two populations to unaggregated γS-crystallin molecules and a

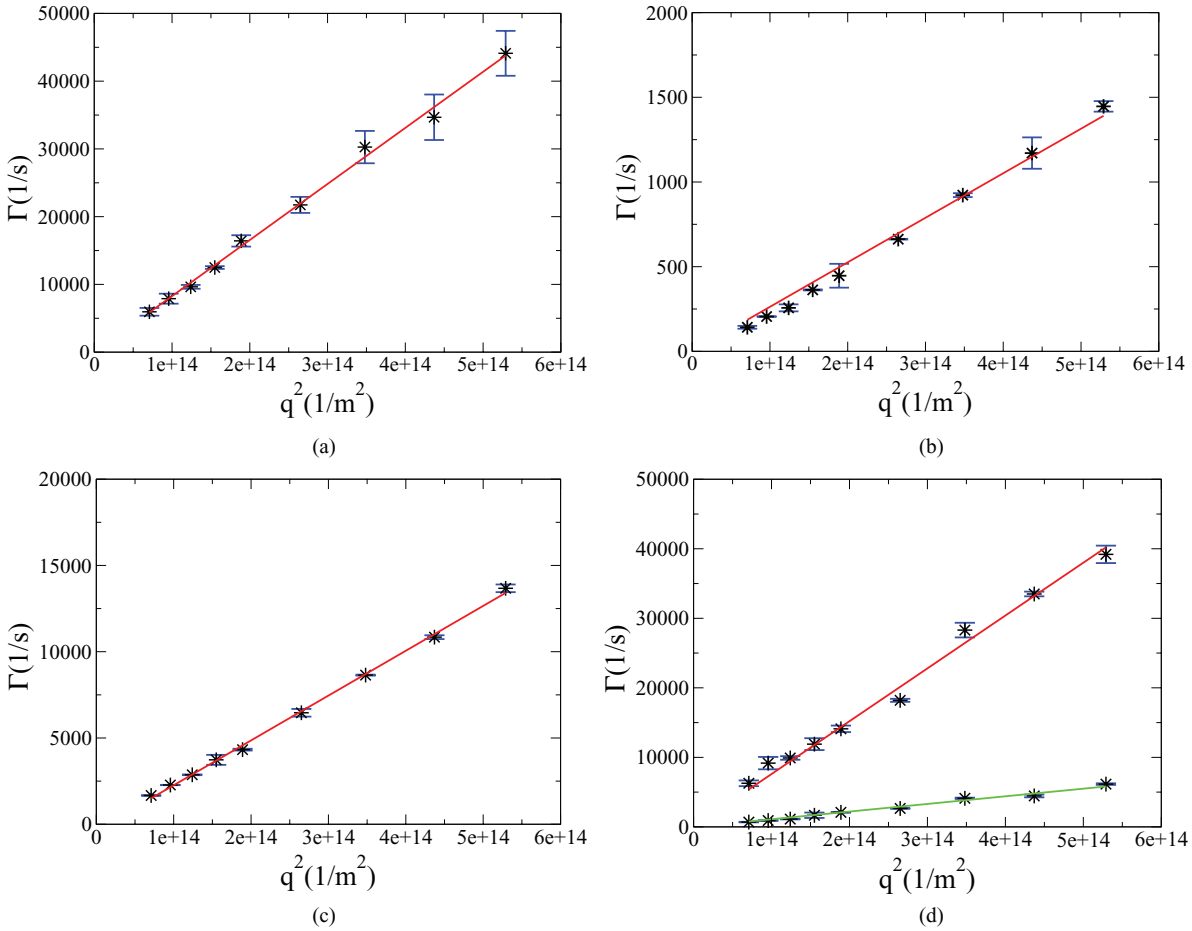

FIG. 3. Linear dependence of the decay rate Γ on q^2. (a) and (b) For γS-crystallin solution corresponding respectively to unaggregated monomer and aggregated clusters. (c) For αB-crystallin solution corresponding to one oligomeric size. (d) For a mixture of γS- and αB-crystallins with the two decay rates corresponding to unaggregated monomer of γS (blue) and oligomeric αB (black). The R^2 for the lines in (a), (b), (c), and (d) are 0.989, 0.975, 0.985, and (0.988 (top), 0.983 (bottom)), respectively.

TABLE I. Hydrodynamic radii corresponding to the faster ($R_{h,f}$) and slower ($R_{h,s}$) modes in solutions containing only the individual components and their mixtures.

Crystallin protein	CONTIN		Multi-exponential	
	$R_{h,f}$ (nm)	$R_{h,s}$ (nm)	$R_{h,f}$ (nm)	$R_{h,s}$ (nm)
γD	2.7 ± 0.2	109 ± 13	3.0	116
γS	2.6 ± 0.2	95 ± 8	3.4	113
αA		13 ± 1		13
αB		8.7 ± 0.5		9.2
$\alpha A \pm \gamma D$	3.1 ± 0.3	17 ± 1	2.8	16
$\alpha A \pm \gamma S$	2.9 ± 0.3	16 ± 2	2.6	13
$\alpha B \pm \gamma D$	2.2 ± 0.2	15 ± 2	2.1	16
$\alpha B \pm \gamma S$	2.9 ± 0.2	16 ± 1	3.6	15

spontaneously aggregated structure made of many γS-crystallin molecules. The R_h value of about 2.6 nm is consistent with the estimated globular size of a protein molecule of 20.6 kDa. The larger size of about 100 nm is clearly nonmonomeric and must correspond to an aggregate of many molecules. Our value for the monomer radius is consistent with the value of 2.5 nm previously reported by Liu *et al.*[43] for bovine γS-crystallin based on light scattering (although estimated based on only one scattering angle). It must be mentioned that Liu *et al.*[43] also observed a slowly developing aggregate of about 10 nm over a period of 97 days. This value is different from ours for the human γS-crystallins. However, in the work of Liu *et al.*,[43] only one scattering angle of 90° was used and the protein concentration was higher at 3 mg/ml. In addition, the pore size of their filter was 220 nm. As shown below, for such higher protein concentrations, the aggregate size (for human crystallins) is above this pore size. In our experiments, the aggregates formed spontaneously at higher protein concentrations were filtered away if we used 0.22 μm fllters.

Based on the present data alone, it is impossible to discern the number of protein molecules constituting the aggregate. However, estimates of this number can be made based on presumed models. Several models for the aggregated structure are conceivable: a closely packed spherical assembly of globular monomers, a rodlike filamental assembly, a polymeric chain of protein monomers with a certain statistics such as the Gaussian or self-avoiding-walk, or a branched architecture similar to a physical microgel. The internal structure of the protein aggregates in our system is unknown at present and needs to be investigated in the future. Since the number of monomers in the aggregate depends sensitively on the particular model for the aggregate, we refrain from making an estimate of this number. Nevertheless, it is absolutely clear that the typical radius of the aggregate is about 40 times larger than the radius of unaggregated monomer.

We have followed exactly the same procedure as above for the solution of γD-crystallin. Again, there are two clearly separated modes (see the supplementary material)[61] corresponding to the unaggregated and aggregated populations. The analysis of the distribution function of decay times and the q-dependence of decay rates, and the use of Stokes-Einstein relation give the two hydrodynamic radii as 2.7 ± 0.2 nm (unaggregated monomer) and 109 ± 13 nm (aggregate), as given in Table I.

B. One oligomeric population in α-crystallin solutions

The DLS measurements on individual solutions of αA- and αB-crystallins revealed a qualitatively different behavior from that of γ-crystallin solutions. The DLS results for a solution of αB-crystallin (with protein concentration of 1.0 mg/ml and 150 mM NaCl at 37 °C and pH 6.8 (20 mM N_2HPO_4/NaH_2PO_4)) are given in Figs. 1–3(c), respectively, for the field correlation function, distribution function of decay times, and q^2-dependence of decay rate. A comparison between the $g_1(t)$ curves in Fig. 1 reveals that the correlation function decays faster for αB-crystallin solution than for the γS-crystallin solution. More significantly, the key result of Fig. 2(b) is that there is only one mode of decay for protein concentration fluctuations showing that there is only one population of αB-crystallin molecules in terms of their size. This is in contrast to the two modes seen in Fig. 2(a) for the γS-crystallin solution. The single mode seen in αB-crystallin solutions obeys the diffusive law as shown in Fig. 3(c).

The hydrodynamic radius inferred from the slope of the line in Fig. 3(c) and the Stokes-Einstein law is 8.7 ± 0.5 nm. The same procedure as above for the solution of αA-crystallin showed that there is only one mode of diffusive mode with the value of 13 ± 1 nm for R_h (Table I) (see the supplementary material).[61] These values are quite high for monomeric protein molecules of molar mass of about 20 kDa, suggesting that α-crystallin molecules exist as oligomers.[10] Similar results were already reported for bovine α-crystallin solutions. In order to explore more on this issue, we analyzed the static light scattering data on solutions of αB- and αA-crystallins. The fact that there is only one mode of concentration fluctuations in the α-crystallin solutions allowed us to analyze the static light scattering data, in contrast to the γ-crystallin solutions. The Zimm plots (of the inverse scattering intensity against q^2 at several protein concentrations c in dilute solutions) are given in Fig. 4. The slopes of the extrapolated lines for $c = 0$ and $q = 0$ and the intercept of these lines gave the radius of gyration R_g, second virial coefficient, and the apparent mass, as 10.7 nm, 3.98×10^{-7} mol cm^3 g^2, and 647 kDa, respectively, for αA. It must be mentioned that we are almost at the limit of correct deduction of R_g values from static light scattering due to the small sizes of the molecules. The corresponding values for αB are 11.1 nm, 6.67×10^{-6} mol cm^3 g^2, and 700 kDa. The ratio of our values of R_g from static light scattering and R_h from DLS is 0.82 for αA-crystallin and 1.2 for αB-crystallin. These values are close to the theoretical value for compact spheres. Based on these observations, we suggest that the α-crystallin molecules exist as essentially compact oligomers. The apparent mass (roughly 700 kDa) obtained from static light scattering on our human α-crystallin solutions is much larger than the molar mass of ~20 kDa, suggesting that these oligomers are made of roughly 35 monomers. Our results are consistent with the previously reported values for α-crystallins in dilute solutions.[10] In our measurements, we did not see any symptom of the presence of either the

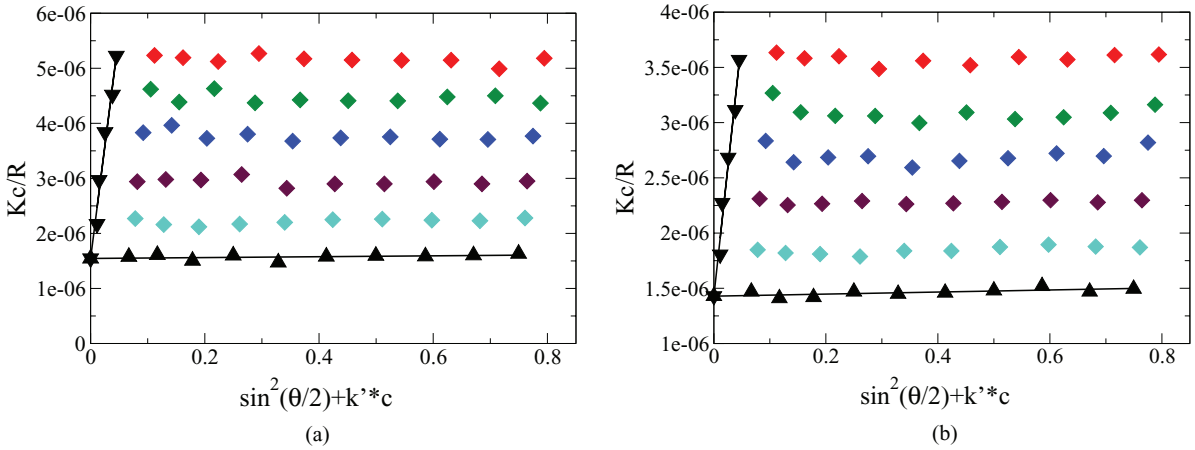

FIG. 4. Zimm plot of inverse scattered intensity (Kc/R) vs. $\sin^2(\theta/2) + k'c$. (a) αA-crystallin solution, and (b) αB-crystallin solution. Protein concentrations are from top to bottom 1.5, 1.28, 0.84, 0.495, and 0.375 mg/ml for (a) and 0.9, 0.77, 0.52, 0.30, and 0.23 mg/ml for (b). ($k' = 10$).

un-oligomerized monomeric α-crystallin molecules or their large clumps. It must be stressed that we see only one population corresponding to the oligomers. We did not see any large scale aggregates in the size range of 100 nm, in contrast to the double population of γ-crystallins (sizes in ~2 nm and ~100 nm). These conclusions are robust and do not depend on whether we use CONTIN or multi-exponential analysis (see below).

C. Deaggregation of γ-crystallin aggregates by α-crystallin

The DLS results of the field correlation function $g_1(t)$, distribution function of delay times, and the q^2-dependence of the decay rates Γ, for the 3:1 mixture of αB- and γS-crystallins are given in Figs. 1, 2(c), and 3(d), respectively. The experimental conditions were 1.5:0.5 mg/ml of αB- to γS-crystallin. The most remarkable result in these figures is that the earmarks of the presence of large aggregates from γS-crystallin are absent in the presence of αB-crystallin. The $g_1(t)$ trace for the mixture decays quicker than that for solutions containing only γS and its behavior is close to that of αB, as revealed by a comparison of the traces in Fig. 1. The distribution function of the decay times for the mixture (Fig. 2(c)) exhibits two modes. If there were no interference between the γS and αB, we should have seen three distinct modes (two from γS, Fig. 2(a), and one from αB, Fig. 2(b)). Instead we saw only two modes. Analysis of these modes, as given in Fig. 3(d), shows that these modes are both diffusive. From the slopes of these two straight lines in Fig. 3(d), the hydrodynamic radii are obtained as 3.0 ± 0.2 nm and 17 ± 2 nm (Table I). These values are close to the monomeric value of γS-crystallin and the oligomeric value of αB-crystallin seen in the unmixed solutions. The slightly higher values seen in the mixture are presumably due to modest levels of mutual binding between the γS monomers and αB oligomers. The DLS is not fine enough to probe such intermolecular interactions inside a complex. However, it is clear that there are no aggregates with R_h in the range of ~100 nm.

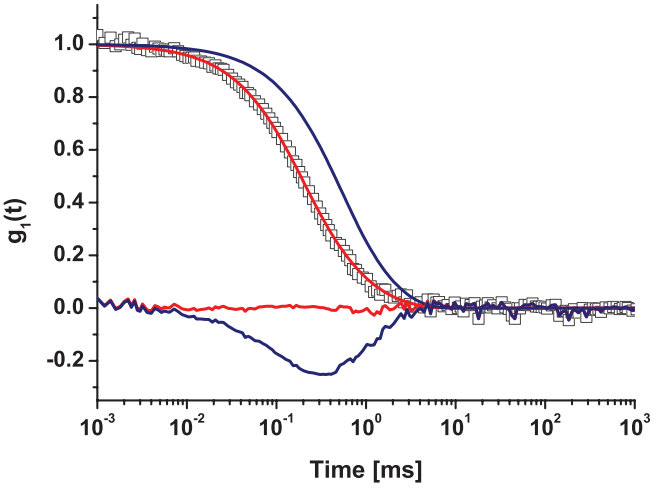

FIG. 5. Multi-exponential fitting of the field correlation function for the mixture of γS and αB. Open squares denote the experimental data. Blue curve is expected result if all three modes (two from γS and one from αB) were to contribute. Red curve is the fit with contributions from αB and the monomeric γS. The curves around $g_1(t) = 0$ are the residuals between the fitted curves (blue and red) and the actual data.

The absence of the third mode corresponding to the aggregated γ-crystallin is additionally verified by analyzing the DLS data with the procedure of Rausch *et al.*[54] The results are given in Fig. 5, as obtained by the following procedure. First, the normalized field correlation function $g_1(t)$ of γS is well described by the sum of two exponentials:

$$g_{1,\gamma} = a_{1,\gamma} \exp\left(-\frac{t}{\tau_{1,\gamma}}\right) + a_{2,\gamma} \exp\left(-\frac{t}{\tau_{2,\gamma}}\right), \qquad (6)$$

where a_i and $\tau_i = 1/q^2 D_i$ represent the amplitude and decay times, respectively. The bi-exponential fit is indicative of two distinct decay times, a result which is easily visualized with the bimodal distribution provided by the CONTIN analysis. Similarly, the normalized field correlation function for αB is fitted by a sum of two exponentials:

$$g_{1,\alpha} = a_{1,\alpha} \exp\left(-\frac{t}{\tau_{1,\alpha}}\right) + a_{2,\alpha} \exp\left(-\frac{t}{\tau_{2,\alpha}}\right). \qquad (7)$$

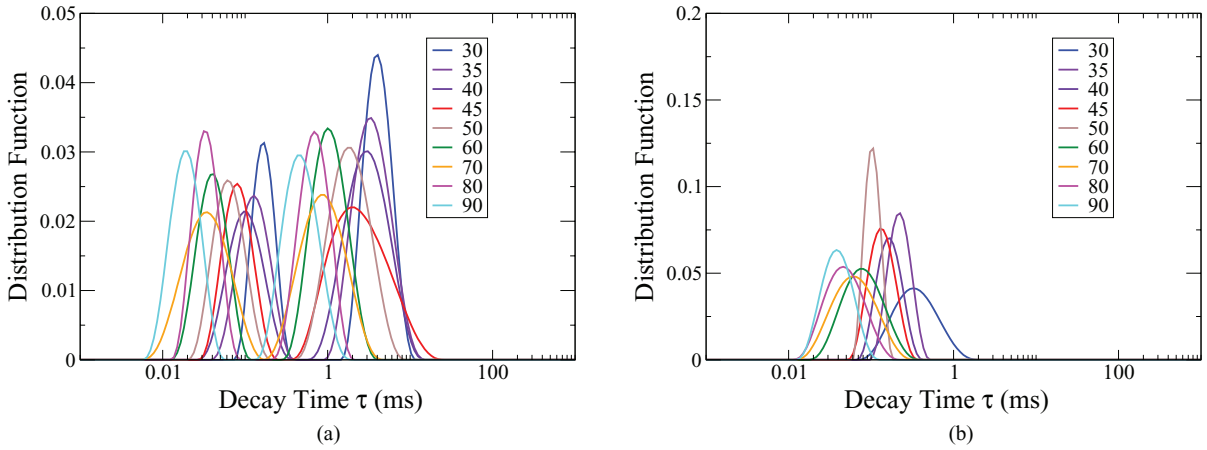

FIG. 6. Distribution function versus decay time at various scattering angles for γS-crystallin solution at NaCl concentrations of (a) 300 mM and (b) 500 mM.

Although a single exponential fit in CONTIN analysis describes this system well, two exponentials are used due to the polydispersity of the oligomers of αB. We believe that it is polydispersity in contrast to two distinctly different sizes, because the CONTIN analysis of this system gives only a single decay. In order to get the hydrodynamic radius, the two decay times are averaged based on their weights to the total scattered intensity. The results for the hydrodynamic radius from the CONTIN analysis and multi-exponential analysis are in agreement (Table I). Next, we analyze the data for the mixture of γS and αB. The correlation function for the mixture $g_{1,m}(t)$ of x and y components is a linear combination of the pure contributions $g_{1,x}(t)$ and $g_{1,y}(t)$,

$$g_{1,m}(t) = f_x g_{1,x}(t) + f_y g_{1,y}(t), \tag{8}$$

where f_x and f_y are the only fitting parameters. The open squares in Fig. 5 are the normalized field correlation functions from experiments $g_{1,m}(t)$. By keeping $g_{1,x}(t)$ and $g_{1,x}(t)$ fixed from the pure component results and fitting only f_x and f_y, the best fit is the blue curve in the figure. The experimental curve is clearly shifted to shorter correlation times. The residual of the forced fit (given by the difference between the data points and the fitted curve) is plotted in blue along the baseline. Clearly there is a substantial negative deviation at longer times. These deviations, complementing the CONTIN analysis, indicate the disappearance of the large aggregates of γS in the mixture. Furthermore, in order to show that monomeric γS is present in the mixture with the oligomeric αB, we fitted $g_{1,m}(t)$ with $g_{1,\alpha}(t)$ and $g_{1,\gamma,fast}(t)$, which corresponds to the monomeric γS,

$$g_{1,m}(t) = f_\alpha g_{1,\alpha}(t) + f_{\gamma,fast} g_{1,\gamma,fast}(t). \tag{9}$$

As shown in Fig. 5, the experimental data can be described by the red curve obtained from the fitted weights. The residual between the fitted red curve and the data is given by the red curve along the baseline. These analyses clearly show that there is no additional aggregate present in the mixture, consistent with the CONTIN analysis.

This conclusion is general for all possible combinations of α and γ, namely, $\alpha A + \gamma D$, $\alpha A + \gamma S$, $\alpha B + \gamma D$, and $\alpha B + \gamma S$. The DLS data for the other three combinations not presented above are given in the supplementary material,[61] and the final results of R_h are given in Table I.

D. Origin of aggregation in γ−crystallins

Having demonstrated the spontaneous formation of aggregates by γ-crystallin molecules in dilute solutions and their demolition by α-crystallin molecules, we proceeded to investigate the response of aggregates to variations in experimental conditions. The primary goal of these investigations *in vitro* was to evaluate the extent of non-covalent forces versus covalent cross-links in controlling the nature of the γ-crystallin aggregates. We have investigated the response of the aggregates to salt concentration, pH, temperature, protein concentration, the reducing agent DTT, and oxidation. We have studied the individual solutions of γD- and γS-crystallins under the same conditions as in Sec. III A. Instead of presenting volumes of data for each of the solutions investigated, we show only a few sets of data and the rest are provided in the supplementary material.[61] Only the key representative results are given below.

1. Effect of salt concentration

The experimental protocol is described in Sec. II and the data analysis is exactly the same as above. We have used NaCl as the salt and the concentration range is 0.1M–1.0M. We found that the salt concentration plays a major role in affecting the aggregation of γ-crystallin. For NaCl concentrations above 400 mM, the large aggregate of γ-crystallin is not seen in DLS. As a typical example, the distribution functions of decay times for γS-crystallin solutions containing 300 mM NaCl and 500 mM NaCl are given in Figs. 6(a) and 6(b), respectively. Even a superficial visual inspection reveals a qualitative change in the distribution functions. There is only one mode for the higher salt concentration and there are two modes for the lower salt concentration (one fast corresponding to monomers, and the other slower mode corresponding to the aggregate). The decay rates of these two modes (at 300 mM NaCl) are plotted against q^2 in Figs. 7(a) and 7(b), respectively. Since only one mode is observed for 500 mM

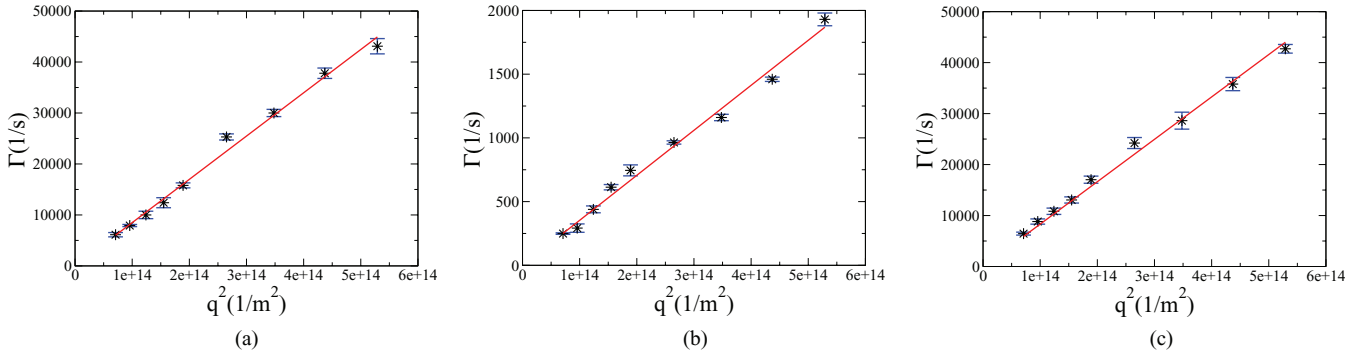

FIG. 7. Linear dependence of the decay rate Γ on q^2 for γS-crystallin solution. (a) and (b) For 300 mM NaCl solution representing faster and slower modes, respectively. (c) For 500 mM NaCl. The R^2 for the lines in (a), (b), and (c) are 0.995, 0.982, and 0.994, respectively.

NaCl, its decay rate versus q^2 is given in Fig. 7(c). The data analysis of these curves gives two hydrodynamic radii, 2.9 ± 0.2 nm and 100 ± 6 nm at 300 mM NaCl, and only one hydrodynamic radius of 2.5 ± 0.1 nm at 500 mM NaCl. Exactly the same trend was observed for solutions of γD-crystallin. The overall data on R_h for γS- and γD-crystallins for various salt concentrations are summarized in Table II. Therefore, the spontaneously aggregated structure from γS-crystallin at lower salt concentrations dissolves as the salt concentration is increased. This is a clear demonstration of electrostatic interactions being the force in holding the γ-crystallin molecules together in their aggregates at lower ionic strengths.

2. Effect of pH

Analogous to the significant role of salt concentration in dictating the presence or absence of the γ-crystallin aggregates, the pH of the solution also plays a major role. Since there are ten lysine residues in the human γS-crystallin sequence, and because the nominal pK_a of the conjugate acid of lysine is about 10.5, we performed DLS measurements on solutions of γS-crystallin at pH of 10 and below, and pH of 11. The distribution functions of decay times for these two pH values are given in Fig. 8. There are two modes (Fig. 8(a)) at pH = 10 and there is only one mode (Fig. 8(b)) at pH = 11. The corresponding decay rates as functions of q^2 are presented in Fig. 9. The results for the two modes at pH = 10 are given in Fig. 9(a) (unaggregated monomer) and Fig. 9(b) (aggregate of γS-crystallin); the result for the single mode at pH = 11 is given in Fig. 9(c). The values of hydrodynamic radii at pH = 10 are 3.4 ± 0.2 nm and 90 ± 7 nm. At pH = 11, the only hydrodynamic radius observed is 3.1 ± 0.1 nm. These results and our measured values at other lower pH values are given in Table III. We have observed a similar effect with solutions of γD-crystallin, except that the aggregate is stable at pH below 10 and unstable at pH = 10 and above. The pH-dependencies of the hydrodynamic radii for γD-crystallin are also included in Table III. It is clear from the data in Table III that electrostatic forces play a role in the formation of aggregates. Since fibers were shown[55,56] to be formed by γ-crystallins at very low pH values of 2 and 3, we stayed away from such low pH conditions in order to avoid any potential interference between the fibrillization and three-dimensional aggregation.

TABLE II. Effect of temperature on hydrodynamic radii in individual αA-, αB-, γD-, and γS-crystallin solutions.

Temp	αA	αB	γD		γS	
(°C)	R_h (nm)	R_h (nm)	$R_{h,f}$ (nm)	$R_{h,s}$ (nm)	$R_{h,f}$ (nm)	$R_{h,s}$ (nm)
4	11 ± 1	8.6 ± 2	3.0 ± 0.2	116 ± 14	3.0 ± 0.1	100 ± 18
22	13 ± 1	8.7 ± 1	2.8 ± 0.1	104 ± 10	2.7 ± 0.4	102 ± 14
37	13 ± 1	9.1 ± 1	2.7 ± 0.2	109 ± 13	2.6 ± 0.3	95 ± 8

3. Effect of temperature

We have performed DLS measurements on individual solutions γD-, γS-, αA-, and αB-crystallins as a function of temperature. The experimental procedure and data analysis are exactly the same as above and we merely provide a summary of the results on the hydrodynamic radius in Table IV for temperatures of 4 °C, 22 °C, and 37 °C. There is only one radius for αA and αB and there are two radii for each of γD and γS. It is seen from Table IV that the temperature does not play a major role in the range of temperature investigated.

4. Effect of protein concentration

By repeating the above described DLS experiments on individual solutions of γD- and γS-crystallins as a function of protein concentration, we have found that the aggregate size increases with protein concentration, whereas the size of the unaggregated monomer remains constant as expected. A summary of our DLS results is provided in Table V. As the protein concentration is increased from 0.5 mg/ml to 4 mg/ml, the hydrodynamic radius increases by about a factor of three from ∼100 nm to ∼300 nm.

5. Effect of a reducing agent

Since there is a huge literature demonstrating the relevance of disulfide bonds in the aggregates of γ-crystallin, we exposed our solutions containing spontaneously formed

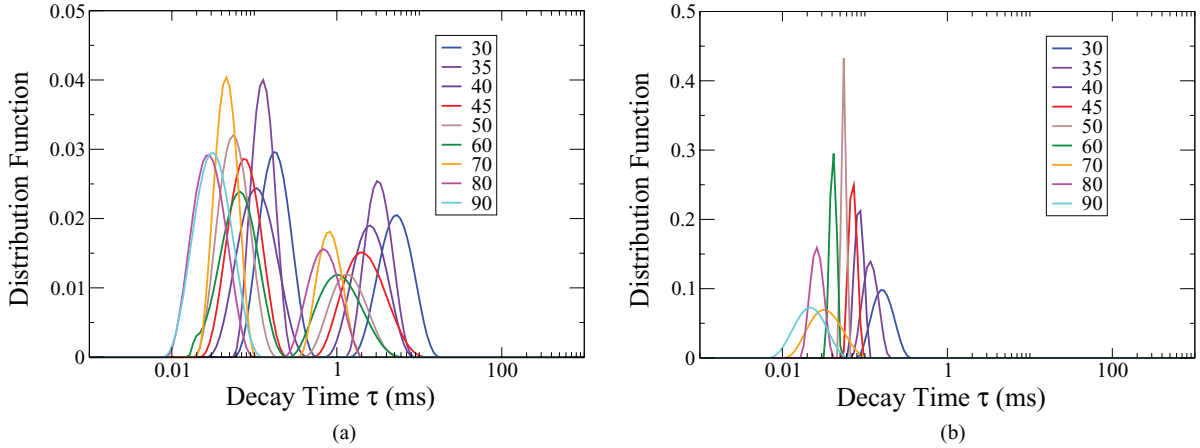

FIG. 8. Distribution function versus decay time at various scattering angles for γS-crystallin solution at (a) pH = 10 and (b) pH = 11.

aggregates to the reducing agent DTT at 1 mM concentration. The experimental protocol is described in Sec. II. The DLS results for the hydrodynamic radii for γD and γS are summarized in Table VI. For the purpose of comparisons, data from Table I in the absence of DTT are also included in Table VI. It is clear from Table VI that the reducing agent does not alter the size of the aggregate, suggesting that the origin of the aggregation in the investigated dilute solutions is not due to covalently formed disulfide bonds between different parts of the protein molecules.

6. Effect of oxidation

Since the reducing agent DTT does not affect the aggregate size, we deliberately exposed the crystallin solutions to oxidizing conditions.

We investigated the effect of the oxidizing agent $CuCl_2$ on the individual solutions of γD- and γS-crystallins (protein concentration = 0.2 mg/ml, $CuCl_2$ concentration = 0.1 mM in 150 mM NaCl and 20 mM phosphate buffer, pH = 6.8). To begin with, the solution in the absence of $CuCl_2$ is subjected to size exclusion chromatography, as described in Sec. II. The chromatogram for the γS- solution is shown in Fig. 10(a). The absorbance at 280 nm showed only one major peak at the elution times of about 39 min. Fractions of 1 ml were collected from the column and subjected to SDS-PAGE analysis. The presence of γS-crystallin was confirmed in the fractions that flowed out in the range of 34–43 min. Molecular weight standards were used to calibrate the relative elusion times. Molecular weights of 17.6 kDa, 66 kDa, 669 kDa, and 2000 kDa corresponded to the elution times of 40, 31.5, 24.5, and 19 min, respectively. Therefore, the peak at about 39 min corresponds to the expected molecular weight of monomeric γS-crystallin (∼21 kDa). It is to be noted that there is only one peak and there is no evidence of the aggregate being excluded from the voids of the column, presumably due to their break-up during the flow. By contrast, the presence of $CuCl_2$ led to an additional peak in the chromatogram as shown in Fig. 10(b). In the presence of $CuCl_2$, we first observed coexistence of a precipitate and a supernatant liquid. The supernatant liquid was then subjected to size exclusion chromatography, as described in Sec. II. In the chromatogram for the γS solution containing the oxidizing agent (Fig. 10(b)), the absorbance at 280 nm showed two major peaks at the elution times of about 39 and 17 min. From the calibration with molecular weight standards mentioned above, the cutoff molecular weight corresponding to the peak at 17 min is in the range of several thousands of kDa, confirming the presence of cross-linked aggregates with mass comparable to or larger than this cutoff value. The primary peak at 38 min corresponds to the expected molecular weight of monomeric γS-crystallin (∼21 kDa).

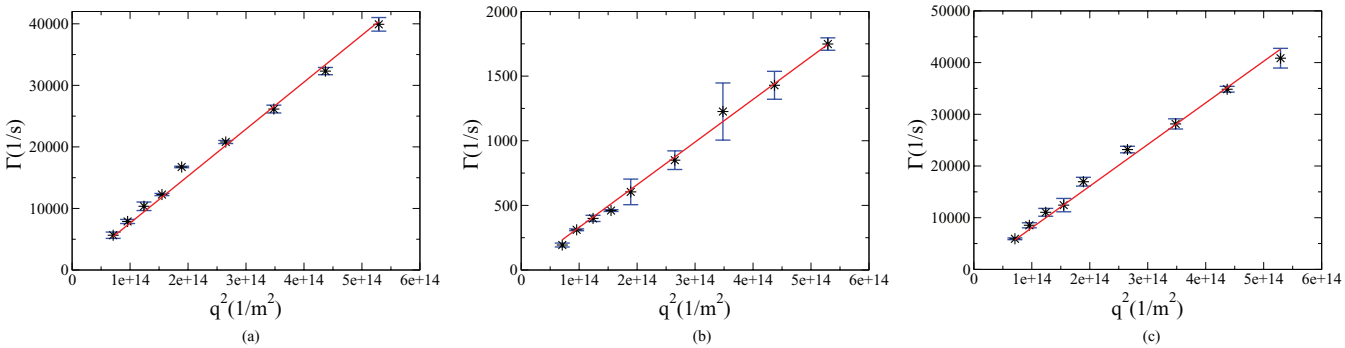

FIG. 9. Linear dependence of the decay rate Γ on q^2 for γS-crystallin solution. (a) and (b) For pH = 10 representing faster and slower modes, respectively. (c) For pH = 11. The R^2 for the lines in (a), (b), and (c) are 0.982, 0.992, and 0.997, respectively.

TABLE III. Effect of protein concentration on aggregate size in γD- and γS-crystallin solutions.

Concentration	γD		γS	
(mg/ml)	$R_{h,f}$ (nm)	$R_{h,s}$ (nm)	$R_{h,f}$ (nm)	$R_{h,s}$ (nm)
0.5	3.1 ± 0.1	98 ± 14	2.7 ± 0.3	90 ± 6
1.0	2.8 ± 0.1	104 ± 10	2.7 ± 0.4	102 ± 14
1.5	2.9 ± 0.2	108 ± 7	2.9 ± 0.1	144 ± 13
2.0	3.0 ± 0.3	155 ± 22	3.1 ± 0.2	162 ± 19
3.0	2.8 ± 0.4	264 ± 18	2.6 ± 0.3	230 ± 19
4.0	3.2 ± 0.5	331 ± 37	3.3 ± 0.5	310 ± 24

TABLE IV. No effect from the reducing agent DTT on the aggregate size.

	γD		γS	
DTT (mM)	$R_{h,f}$ (nm)	$R_{h,s}$ (nm)	$R_{h,f}$ (nm)	$R_{h,s}$ (nm)
0	2.7 ± 0.2	109 ± 13	2.6 ± 0.2	95 ± 8
5	2.6 ± 0.3	108 ± 13	3.0 ± 0.4	102 ± 9

TABLE V. Effect of NaCl concentration on the hydrodynamic radii corresponding to the faster ($R_{h,f}$) and slower ($R_{h,s}$) modes in solutions containing γD- and γS-crystallins separately.

Salt concentration	γD		γS	
(mM NaCl)	$R_{h,f}$ (nm)	$R_{h,s}$ (nm)	$R_{h,f}$ (nm)	$R_{h,s}$ (nm)
100	2.8 ± 0.4	108 ± 13	2.7 ± 0.3	104 ± 12
150	2.8 ± 0.1	104 ± 13	2.7 ± 0.4	102 ± 14
300	2.6 ± 0.2	91 ± 13	2.9 ± 0.2	100 ± 6
400	2.7 ± 0.1	...	2.6 ± 0.3	...
500	2.8 ± 0.2	...	2.5 ± 0.1	...
1000	2.5 ± 0.1	...	2.6 ± 0.3	...

TABLE VI. Effect of pH on the hydrodynamic radii corresponding to the faster ($R_{h,f}$) and slower ($R_{h,s}$) modes in solutions containing γD- and γS-crystallins separately.

	γD		γS	
pH	$R_{h,f}$ (nm)	$R_{h,s}$ (nm)	$R_{h,f}$ (nm)	$R_{h,s}$ (nm)
5	3.9 ± 0.5	100 ± 9	4.8 ± 0.4	141 ± 7
6	2.7 ± 0.3	118 ± 12	2.5 ± 0.3	110 ± 8
8	2.9 ± 0.2	102 ± 16	3.0 ± 0.2	96 ± 11
9	3.5 ± 0.4	97 ± 8	2.9 ± 0.3	106 ± 14
10	3.2 ± 0.3	...	3.4 ± 0.2	90 ± 7
11	3.1 ± 0.2	...	3.1 ± 0.1	...

As a further demonstration of the fact that the spontaneously formed aggregate of γ-crystallin molecules is not covalently cross-linked to begin with, but gets cross-linked as a function of time upon exposure to an oxidizing agent, we have monitored the role of air oxidation. We collected the solution of γS-crystallin after the first elusion, which was air oxidized for several days. This aged solution was then subjected to size exclusion chromatography. The resultant chromatogram after 96 h is shown in Fig. 10(c). It is clear that a new peak around the flow time duration of 11–19 min has developed. As in the presence of $CuCl_2$ (Fig. 10(b)), this new peak corresponds to a covalently cross-linked aggregate.

IV. CONCLUSIONS

We have performed *in vitro* dynamic light scattering measurements on dilute solutions containing human αA-, αB-, γD-, and γS-crystallins under phosphate buffer conditions. The data show the spontaneous formation of clusters with hydrodynamic radii of about 100 nm in solutions containing either γD- or γS-crystallin in addition to unaggregated monomers. The αA- and αB-crystallin solutions show only one population of oligomers with some polydispersity. In mixtures of γ- and α-crystallins, the large aggregates seen in solutions containing only γ-crystallin are absent. The mixtures contain only the unaggregated γ-crystallin monomers and oligomers of α-crystallin molecules.

The status of the aggregates in γ-crystallin solutions depends sensitively on salt concentration and pH. At higher monovalent salt concentrations, with the resultant screening of electrostatic interactions, the aggregates are absent. In addition, when the pH is kept higher so that there is a net negative charge of γ-crystallin, the aggregates are absent due to interchain repulsive forces. Variations in temperature do not affect the aggregate sizes significantly. However, as the protein concentration increases, the size of the aggregate increases. Further, presence of the reducing agent DTT does not alter the size of the aggregate. All of our data converge to the conclusion that the spontaneous aggregation of γ-crystallin molecules is electrostatically driven.

The experimental conditions in the present *in vitro* study are far away from any coexistence curve that could arise in the context of cold cataract.[3,26–30] The aggregates observed here appear to be unrelated to any concentration fluctuations near

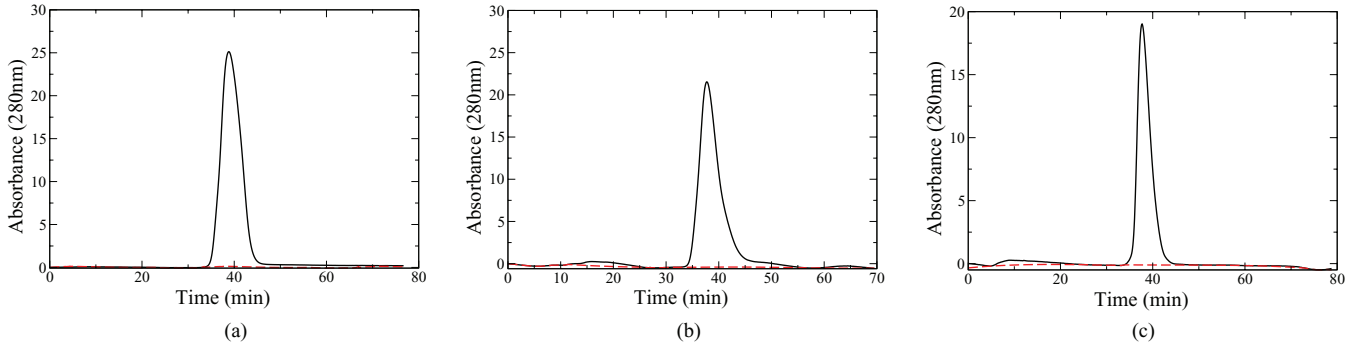

FIG. 10. Chromatogram for γS-crystallin solution: (a) absence of $CuCl_2$ and (b) with 0.1 mM $CuCl_2$. (c) After 4 days of air oxidation.

any potential phase separation phenomenon, as the aggregate size is insensitive to changes in temperature (whereas the correlation length near a critical temperature depends on temperature sensitively[58,59]). The relationship between the formation of aggregates by charged macromolecules at higher temperatures and the concentration fluctuations at lower temperatures is not yet established and continues to be a challenging issue.[60] In the present context, it is of interest to explore the critical phenomenon of human γ-crystallins by considering much higher concentrations and lower temperatures.

For monitoring such large clusters of crystallin proteins in dilute solutions, DLS appears to be a good tool. The sensitivity of DLS allows the monitoring of the size and stability of γ-crystallin aggregates in dilute buffer solutions arising from weak electrostatic forces. The primary result of the present work is that the sensitive DLS shows the spontaneous formation of γ-crystallin aggregates with about 100 nm radius and that these aggregates are destabilized by α-crystallin and enhanced levels of monovalent salt concentration and pH. Extensions of the present work on native crystallins *in vivo* would be of great interest in establishing the relevance of the current results for *in vivo* situations.

The observed importance of ionic interactions among γ-crystallin molecules suggests that these ionic interactions might play an important role in establishing the refractive index gradient in the lens. Crystallins nearer the lens periphery (the lens cortex) are at lower concentrations than those in the deeper fiber cells (the lens nucleus). Changes in intracellular ion concentrations leading to altered protein aggregation could contribute to these gradients, which are important in the lens for reducing spherical aberration. To date, there is little information available about the origin of these protein gradients. Extensions of the present work could lead to a better understanding of protein gradients in lens development.

Our identification that the aggregation in dilute γ-crystallin solutions is essentially driven by noncovalent electrostatic forces might stimulate new strategies to modify the electrostatic potential around the protein molecules in order to suppress their aggregation. Analogous to the case of γ-crystallin aggregation, it is likely that electrostatics might be a significant contributor to the disease-causing aggregation of other proteins as well.

ACKNOWLEDGMENTS

It is a pleasure to thank Professor Jonathan King of MIT for kindly providing the recombinant plasmids of crystallins. The authors are grateful to Kristin Rausch and Professor Manfred Schmidt for discussions regarding data analysis. Acknowledgment is made to Johnson & Johnson Vision Care for supporting this research, National Science Foundation (Grant No. DMR-1105362), and the Materials Research Science and Engineering Center at the University of Massachusetts, Amherst. C.M.D. and S.C.G. acknowledge support from the NIH (R01-DK76877).

[1]C. W. Oyster, *The Human Eye: Structure and Function* (Sinauer Associates Inc., Sunderland, MA, 1999).
[2]S. K. West and C. T. Valmadrid, Surv. Ophthalmol. **39**, 323 (1995).
[3]G. B. Benedek, Invest. Ophthalmol. Visual Sci. **38**, 1911 (1997).
[4]Z. Ma, S. R. Hanson, K. J. Lampi, L. L. David, D. L. Smith, and J. B. Smith, Exp. Eye Res. **67**, 21 (1998).
[5]J. Graw, Exp. Eye Res. **88**, 173 (2009).
[6]C. Slingsby and N. Clout, Eye **13**, 395 (1999).
[7]H. O. Sandberg and O. Closs, Exp. Eye Res. **28**, 601 (1979).
[8]W. W. de Jong, G. J. Caspers, and J. A. Leunissen, Int. J. Biol. Macromol. **22**, 151 (1998).
[9]T. H. MacRae, Cell. Mol. Life Sci. **57**, 899 (2000).
[10]S. P. Delbecq and R. E. Klevit, FEBS Lett. **587**, 1073–1080 (2013), see http://dx.doi.org/10.1016/j.febslet.2013.01.021.
[11]R. Jaenicke, Prog. Biophys. Mol. Biol. **71**, 155 (1999).
[12]I. A. Mills, S. L. Flaugh, M. S. Kosinski-Collins, and J. A. King, Protein Sci. **16**, 2427 (2007).
[13]H. Bloemendal, W. de Jong, R. Jaenicke, N. H. Lubsen, C. Slingsby, and A. Tardieu, Prog. Biophys. Mol. Biol. **86**, 407 (2004).
[14]U. P. Andley, Prog. Retin Eye Res. **26**, 78 (2007).
[15]J. Graw, Prog. Retin Eye Res. **18**, 235 (1999).
[16]F. Skouri-Panet, F. BonnetÃ©, K. Prat, O. Bateman, N. Lubsen, and A. Tardieu, Biophys. Chem. **89**, 65 (2001).
[17]V. N. Lapko, D. L. Smith, and J. B. Smith, Biochemistry **41**, 14645 (2002).
[18]R. J. W. Truscott, Exp. Eye Res. **80**, 709 (2005).
[19]P. G. Hains and R. J. W. Truscott, Invest. Ophthalmol. Visual Sci. **51**, 3107 (2010).
[20]M. G. Friedrich and R. J. W. Truscott, Invest. Ophthalmol. Visual Sci. **51**, 5145 (2010).
[21]J. Horwitz, Exp. Eye Res. **76**, 145 (2003).
[22]R. Jaenicke, FASEB J. **10**, 84 (1996).
[23]M. Beissinger, K. Rutkat, and J. Buchner, J. Mol. Biol. **289**, 1075 (1999).
[24]M. Wenk, R. Herbst, D. Hoeger, M. Kretschmar, N. Lubsen, and R. Jaenicke, Biophys. Chem. **86**, 95 (2000).
[25]S. R. Hanson, A. Hasan, D. L. Smith, and J. B. Smith, Exp. Eye Res. **71**, 195 (2000).
[26]M. Delaye, J. I. Clark, and G. B. Benedek, Biochem. Biophys. Res. Commun. **100**, 908 (1981).
[27]M. Delaye, J. I. Clark, and G. B. Benedek, Biophys. J. **37**, 647 (1982).
[28]J. I. Clark, J. R. Neuringer, and G. B. Benedek, J. Gerontol. **38**, 287 (1983).
[29]J. I. Clark, T. B. Osgood, and S. J. Trask, Exp. Eye Res. **45**, 961 (1987).
[30]J. I. Clark and D. Carper, Proc. Natl. Acad. Sci. U.S.A. **84**, 122 (1987).
[31]J. A. Jedziniak, J. M. Kinoshita, E. M. Yates, L. O. Hokker, and G. B. Benedek, Invest. Ophthalmol. Visual Sci. **11**, 905 (1972).
[32]J. I. Clark, L. Meugel, A. Bagg, and G. B. Benedek, Exp. Eye Res. **31**, 399 (1980).
[33]J. I. Clark and M. E. Danford, Ophthalmic Res. **17**, 246 (1985).
[34]M. Delaye, M. E. Danford-Kaplan, J. I. Clark, B. Krop, T. Gulik-Krzywicki, and A. Tardieu, Exp. Eye Res. **44**, 601 (1987).
[35]J. Horwitz, Proteins **89**, 10449 (1992).
[36]B. Raman and C. M. Rao, J. Biol. Chem. **269**, 27264 (1994).
[37]K. Wang and A. Spector, Invest. Ophthalmol. Visual Sci. **36**, 311 (1995).
[38]U. P. Andley, S. Mathur, T. Griest, and J. M. Petrash, J. Biol. Chem. **271**, 31973 (1996).
[39]P. J. Muchowski, J. A. Bassuk, N. H. Lubsen, and J. I. Clark, J. Biol. Chem. **272**, 2578 (1997).
[40]J. I. Clark and P. J. Muchowski, Curr. Opin. Struct. Biol. **10**, 52 (2000).
[41]A. Tardieu, F. Veretout, B. Krop, and C. Slingsby, Eur. Biophys. J. **21**, 1 (1992).
[42]J. Xia, T. Aerts, K. Donceel, and J. Clauwaert, Biophys. J. **66**, 861 (1994).
[43]C. Liu, J. Pande, A. Lomakin, O. Ogun, and G. B. Benedek, Invest. Ophthalmol. Visual Sci. **39**, 1609 (1998).
[44]O. Ox, B. K. Derham, and J. J. Harding, Progress in Retinal and Eye Research **18**, 463–509 (1999).
[45]B. K. Derham, M. A. van Boekel, P. J. Muchowski, J. I. Clark, J. Horwitz, H. W. Hepburne-Scott, W. W. de Jong, M. J. Crabbe, and J. J. Harding, Eur. J. Biochem. **268**, 713 (2001).
[46]L. Acosta-Sampson and J. King, J. Mol. Biol. **401**, 134 (2010).
[47]P. Das, J. King, and R. Zhou, Proc. Natl. Acad. Sci. U.S.A. **108**, 10514 (2011).
[48]K. L. Moreau and J. King, PLoS ONE **7**, e37256 (2012).
[49]K. L. Moreau and J. King, Trends Mol. Med. **18**, 273 (2012).
[50]A. Pande, J. Pande, N. Asherie, A. Lomakin, O. Ogun, J. King, N. H. Lubsen, D. Walton, and G. B. Benedek, Proc. Natl. Acad. Sci. U.S.A. **97**, 1993 (2000).
[51]B. Chu, *Laser Light Scattering* (Academic Press, Boston, 1991).
[52]B. J. Berne and R. Pecora, *Dynamic Light Scattering* (Dover Publications, New York, 1976).

[53]P. Stepanek, in *Dynamic Light Scattering*, edited by W. Brown (Clarendon Press, Oxford, 1993).
[54]K. Rausch, A. Reuter, K. Fischer, and M. Schmidt, Biomacromolecules **11**, 2836 (2010).
[55]K. Papanikolopoulou, I. Mills-Henry, S. L. Thol, Y. Wang, A. A. R. Gross, D. A. Kirschner, S. M. Decatur, and J. King, Mol. Vis **14**, 81 (2008).
[56]Y. Wang, S. Petty, A. Trojanowski, K. Knee, D. Goulet, I. Mukerji, and J. King, Invest. Ophthalmol. Visual Sci. **51**, 672 (2010).
[57]X. W. Wang and F. A. Bettelheim, Proteins **5**, 166 (1989).
[58]V. M. Prabhu, M. Muthukumar, G. D. Wignall, and Y. B. Melnichenko, Polymer **42**, 8935 (2001).
[59]V. M. Prabhu, M. Muthukumar, G. D. Wignall, and Y. B. Melnichenko, J. Chem. Phys. **119**, 4085 (2003).
[60]S. Kanai and M. Muthukumar, J. Chem. Phys. **127**, 244908 (2007).
[61]See supplementary material at http://dx.doi.org/10.1063/1.4816367 for light scattering data on γ- and α-crystallin mixtures.